Structural and dielectric studies of $Ni_{1-x}Al_xFe_2O_4$

Sunny Choudhary,[1, a)] Deepanshi Singh,[2] Mohan Bhattarai,[1] Ram S Katiyar,[1] and Poonam Kumari[3]

[1)]*Department of Physics, University of Puerto Rico, San Juan, PR-00925, USA*
[2)]*CCS University, Meerut, UP, India*
[3)]*Eternal University, HP, India*

[a)] *Corresponding author: souryabhardwaj@gmail.com*

Abstract.
The nanoparticles of $Ni_{1-x}Al_xFe_2O_4$ ($x = 0, 0.5$) were synthesized via using sol-gel route and studied the structural and dielectric effect of aluminium content on Nickel site. The X-ray diffraction (XRD) revealed the single-phase cubic spinel structure of the parent compound. The lattice constant, volume, density, bond lengths, specific surface area and crystallite size were determined from the Rietveld refinement. In the Raman analysis, there are five active modes present in the synthesized samples. FTIR spectroscopy confirmed the formation of spinel ferrite and showed the characteristics absorption bands of metal oxygen (Fe-O) observed around 424-450 and 601-620 cm^{-1} corresponding to the stretching vibration frequency of the metal-oxygen at the octahedral site and tetrahedral site respectively. Dielectric behaviour showed that the value of dielectric constant (ε') and tangent loss ($\tan\delta$) decreases with frequency and confirmed the general behaviour of ferrites. The AC Conductivity (σ_{ac}) was found lower in $Ni_{0.5}Al_{0.5}Fe_2O_4$ compared to $NiFe_2O_4$.

1. INTRODUCTION

In recent years, magnetic nanoparticles have garnered significant attention due to their wide-ranging utility in technological and clinical contexts [1]. Within this domain, ferrospinels constitute a prominent class of magnetic materials, exhibiting a diverse spectrum of applications spanning from low wavenumber to microwave frequencies, as well as across low to high permeability devices. These applications encompass areas such as electronics, ferrofluids, magnetic drug delivery, and high-density information storage [2, 3]. The general compositional chemical formula for spinels is AB_2X_4, where A^{2+} is a divalent cation, which might be Mg, Cr, Mn, Fe, Co, or Ni; B^{3+} is a trivalent cation, that can be Al, Ga, In, Ti, or V; and X may be O, S, Se etc.

Nickel ferrite ($NiFe_2O_4$) possesses a crystalline structure distinguished by its cubic inverse spinel configuration. This arrangement features oxygen atoms organized in a cubic close-packed pattern. Within this framework, both divalent metal ions (A), exemplified by nickel (Ni), and trivalent metal ions (B), such as iron (Fe), concurrently occupy positions in both the tetrahedral and oc-

tahedral sites within the unit cell. The unit cell encompasses a total of 32 oxygen atoms, orderly arranged in a cubic close-packed configuration, encompassing 8 tetrahedral sites and 16 octahedral sites that are occupied. The predilection of a cation for occupying A or B sites is primarily contingent on the cation's size [4, 5].
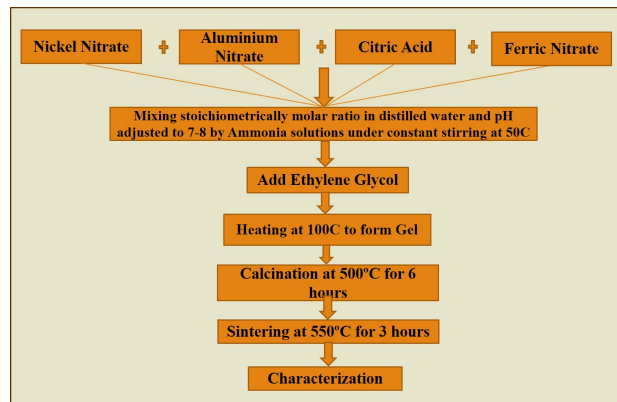

FIGURE 1. The flow chart of the sample preparation by sol-gel method.

Diverse methodologies have been employed to synthesize nickel ferrite nanoparticles, including hydrothermal synthesis, solvothermal synthesis, co-precipitation, combustion techniques, and sol-gel auto-combustion approaches [6]. Notably, the sol-gel auto-combustion technique has been employed for the creation of ultrafine nanoparticles. This method offers several advantages over alternative synthesis techniques, including rapidity, low external energy demand, a simplified one-step process, and the generation of homogeneous crystalline nanoparticles [7]. Throughout the previous decade, concentrated efforts have been channelled toward the enhancement of the dielectric properties of high-magnetization ferrites. These endeavors seek to extend their utility in scenarios demanding high-frequency functionality, such as in the domains of radars, isolators, and circulators. Within this framework, our research has particularly honed in on the integration of nickel and aluminium substitutions into nickel ferrites [8, 9]. Nickel ferrites hold a paramount role as magnetic materials, with their significance stemming from their widespread adoption in microwave apparatuses engineered for operation at elevated frequencies. This choice is motivated by their advantageous attributes of heightened resistivity and minimized losses [9, 10]. The strategic introduction of non-magnetic ions realized through substitution at the Fe sites, provides a mechanism to exert control over the properties of spinel ferrites [11]. Especially in the realm of radio and microwave frequencies, the replacement of aluminium within nickel ferrites demonstrates its adaptability, playing a pivotal role in curbing both electrical and magnetic losses. Furthermore, the incorporation of Al^{3+} ions functions to impede the growth of grains and amplify the mechanical durability of the ferrite materials. Notably, these nickel ferrites with aluminium substitutions exhibit heightened electrical resistivity, which subsequently translates into a tangible reduction in losses attributed to both dielectric effects and eddy currents [9]. Acknowledging the profound importance of Al-substituted $NiFe_2O_4$, the present research embarks upon an exhaustive and comprehensive exploration. It will give us a comparative study for parent nickel ferrite over Aluminium substitution nickel ferrite. In mixed-metal spinel ferrites like $Ni_{1-x}Al_xFe_2O_4$, Equimolar 50% substitution on Nickel site is crucial for studying the cation distribution in the crystal lattice. It helps in understanding how different cations are distributed among the octahedral and tetrahedral sites in the spinel structure.

The present study focuses on the structural and dielectric properties of Al^{3+} ion substitution $NiFe_2O_4$ spinel ferrite systems prepared by a sol-gel auto-combustion method. The Rietveld refinement of XRD suggests the cubic phase with $Fd\bar{3}m$ which also corroborates the analysis of Raman spectra. The frequency-dependent dielectric analysis shows the more stable dielectric constant (ε') on varying frequencies and lower dielectric loss ($\tan\delta$).

2. EXPERIMENTAL

The flow chart of the experimental method is shown in Figure 1. The stoichiometric ratio $Ni_{1-x}Al_xFe_2O_4$ ($x = 0, 0.5$) was chosen and followed the sol-gel auto-combustion method to prepare nanopowder. Nickel nitrate [$Ni(NO_3)_2.6H_2O$] and iron nitrate [$Fe(NO_3)_3.9H_2O$] were dissolved in double distilled water and added 20g of citric acid ($C_6H_8O_7.H_2O$) to synthesize $NiFe_2O_4$ and followed the same procedure while synthesizing the $Ni_{0.5}Al_{0.5}Fe_2O_4$. We used Aluminium nitrate [$Al(NO_3)_2$ $6H_2O$], precursor and same precursor Nickel nitrate, and iron nitrate. The next stage was neutralization of the solution by adding ammonium hydroxide and the addition of ethylene glycol to the solution with continuous stirring as a chelating agent until pH 7. Evaporation of the solution at a temperature 100^0C due to which the highly viscous gel was formed. The fine powder was obtained and calcinated at 500^0C for 6 hours followed by sintering at 550^0C for 3 hours. In the present work, X-ray diffraction (XRD), Raman spectroscopy, Fourier transformation infrared spectroscopy (FTIR), and dielectric measurement are used to study the structural and dielectric behavior of prepared samples.

3. RESULTS AND DISCUSSION

3.1 X-ray Diffraction Analysis

Figure 2(a) shows the XRD pattern of $Ni_{1-x}Al_xFe_2O_4$ ($x= 0.0$ and 0.5). The major diffracted peaks were obtained at 30.29^0, 35.67^0, 37.32^0, 43.36^0, 53.80^0, 57.36^0 and 62.99^0 which found to match with the JCPDS reference code number 01-074-1913 of $NiFe_2O_4$ and the reported data available in recent literature [12, 13]. In the doped sample of nickel ferrite, a small peak is observed at $\sim 33^0$ which might be attributed from Fe_2O_3 which shown as in the inset of Figure 2(a) [14, 15].

TABLE I. Extracted Parameters from the Rietveld Refinement of $NiFe_2O_4$.

Atoms (Wyckoff Positions)	X	Y	Z
Fe^{+2} (8a)	0.125	0.125	0.125
Fe^{+3}/Ni^{+2} (16d)	0.500	0.500	0.500
O (32e)	0.255	0.255	0.255

We observed a progressive shift of peaks toward a higher angle in the Al-substituted sample (Figure 2 (b)), which might be possible due to the difference in the ionic radii of the Ni^{2+} (0.69 Å) and of Al^{2+} (0.51 Å) [16].

Further, XRD data was processed Rietveld refinement (Figure 3) and matched well with $Fd\bar{3}m$ space group symmetry. The Wyckoff Positions (Table 1) and other fitting
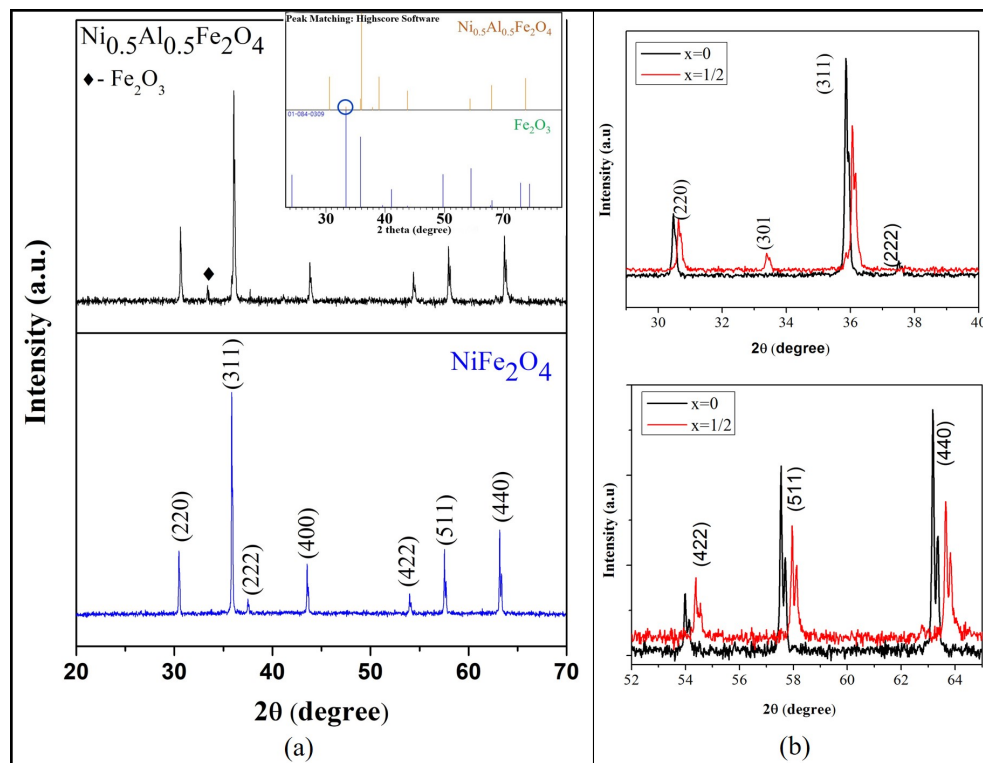
FIGURE 2. (a) XRD pattern of prepared samples. (Inset: XRD pattern of Fe_2O_3 reported in JCPDS data extracted from the X'pert High Score); (b) Peak shifting in comulative mode of origin of the prepared samples
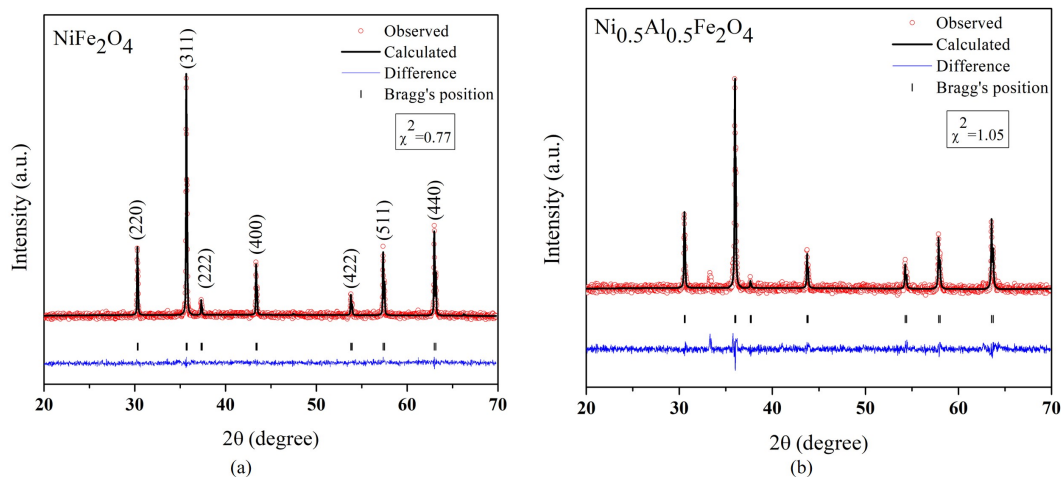

FIGURE 3. Rietveld refined XRD Pattern for x (a) 0.0, and (b) 0.50 doping of Al content

TABLE II. Table of Rietveld refinement parameters.

Sample/Parameters	R_p	R_{wp}	R_{exp}	χ^2
X=0	1.46	1.85	2.11	0.77
X=0.50	1.64	2.15	2.10	1.05

parameters are summarized in Table 2.

The goodness of fit ($\chi^2 \sim 1$) [17, 18], and values of other reliability factors such as R_p, R_{wp}, and R_{exp} validate Rietveld refinement and support the cubic inverse spinel structure. R_p, R_{wp}, and R_{exp} of refinement residuals are utilized to evaluate the accuracy of the correspondence between the observed and computed diffraction patterns,
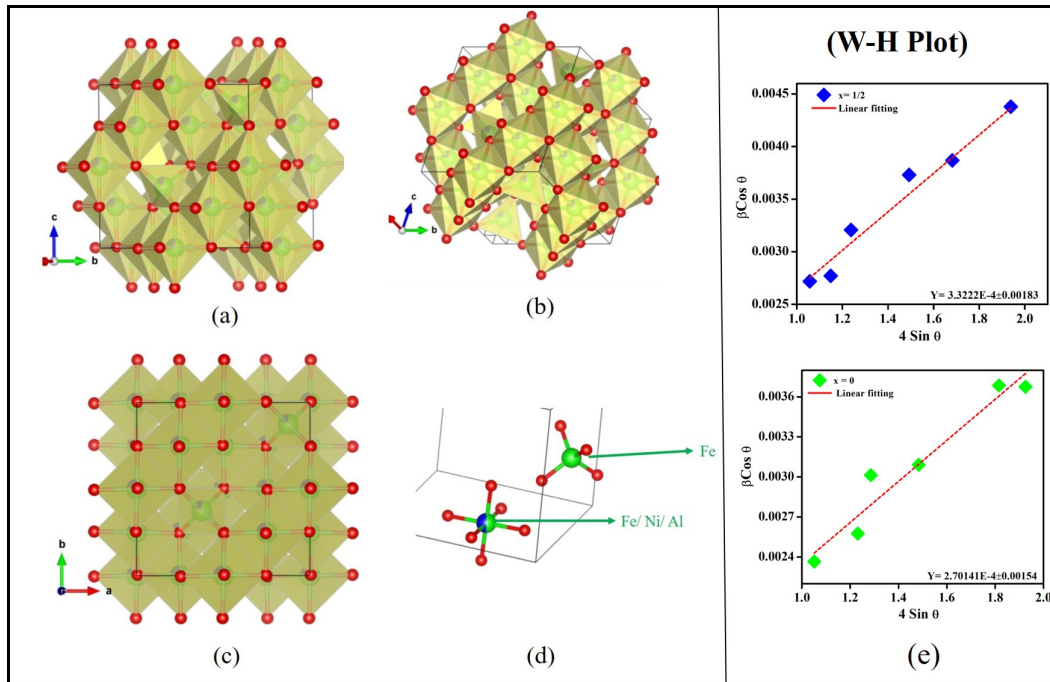
FIGURE 4. Crystal structure extract from the refinement data plotted using Vesta software in various mode (a) polyhedral, (b) reflective, (c) ball and stick (d) individual atomic coordination; (e) Williamson-Hall Plot of $Ni_{1-x}Al_xFe_2O_4$

and the residuals serve as a quantitative measure of the degree to which the model aligns with the empirical data.

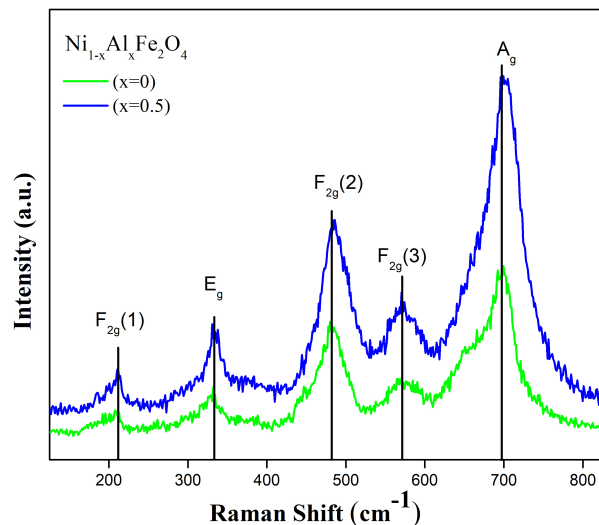**FIGURE 5.** Raman spectra of $Ni_{1-x}Al_xFe_2O_4$ ($x = 0, 0.5$) ferrite.

To visualize, we generated the crystal structure using Vesta software in polyhedral, reflective, ball, and stick mode as shown in Figure 4 (a-c) From the extracted CIF file in Rietveld refinement. The green colour denotes the atoms of Fe^{2+}/Fe^{3+}, blue denotes Ni/Al, and red is for the O- atoms. One can observe from Figure 4 (d) that, Fe^{2+} is coordinated with 4 oxygen atoms forming tetrahedral geometry while Fe^{3+} is coordinated with 6 oxygen atoms forming octahedral. Lattice constant ($a = b = c$), bond lengths between the atoms, crystallite size, density, and volume of the unit cell were found to decrease in $x = 0.5$ as compared to the parent sample of nickel ferrite ($x = 0$) (Table 3). The observed decrease in lattice constant and unit cell volume might be related to the difference in ionic radii. We observed the maximum change in the unit cell lattice parameter and volume to be 0.8% and 2.6% respectively.

Table 3 also illustrates the degree of separation between Ni-O, Fe-Fe, Ni-Ni, and Fe-O crystals changes as the amount of Al substitution [19]. X-ray density (ρ_x) for the prepared ferrites (Table 3) were calculated from the molecular weight and volume of the unit cell for a full range of compositions are found 5.364 g/cc and 5.189 g/cc respectively. The variation of X-ray density with composition is decreased with the Al^{3+} substitution. The decrease in ρ_x is attributed to the decrease in molecular weight of the samples with Al^{3+} substitution [16, 20].

We used Equation 1 [21] and determined the crystallite size of the sample. Figure 4(e) shows the Williamson-Hall (W-H) plot for $NiFe_2O_4$ and $Ni_{0.5}Al_{0.5}Fe_2O_4$.

$$\beta \cos\theta = \frac{K\lambda}{D} + 4\varepsilon_0 \sin\theta \qquad (1)$$

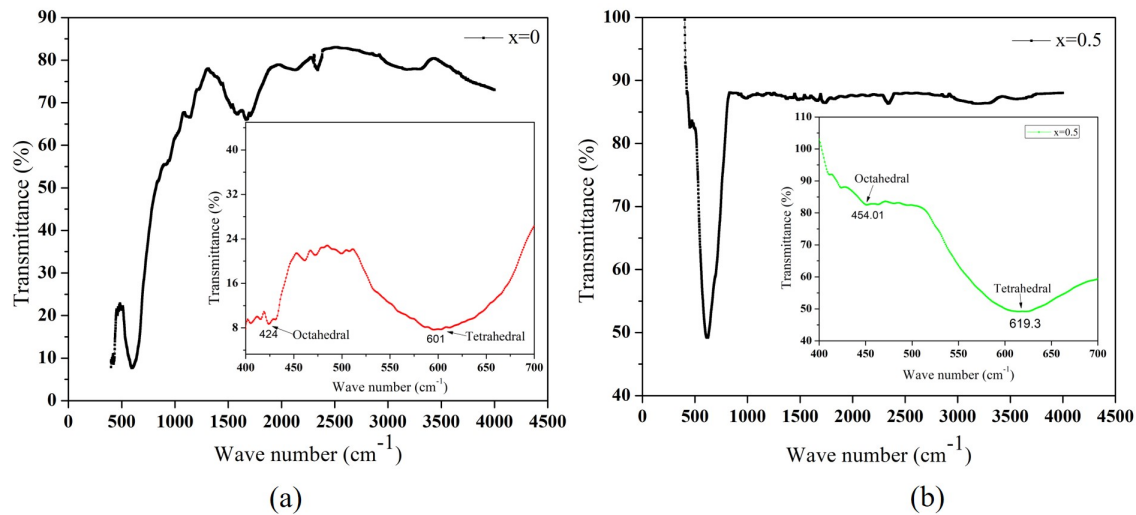**FIGURE 6.** FTIR spectra of synthesized $Ni_{1-x}Al_xFe_2O_4$ (a) $x = 0$, (b) $x = 0.5$.

This plot ascertains the presence of positive strain or tensile strain in the samples, and the crystallite size of $Ni_{0.5}Al_{0.5}Fe_2O_4$ is less than $NiFe_2O_4$. [22] The calculated parameters of the W-H plot are listed in Table 3.

3.2 Raman Spectroscopy

Further, we recorded Raman spectra of $Ni_{1-x}Al_xFe_2O_4$ (x= 0.0 and 0.5) ferrite at room temperature and analyzed the vibrational active modes. The Raman mode of the sample exhibits an inverse spinel structure with prototype symmetry O^{7h} and a space group of $Fd\bar{3}m$. According to group theory, spinel ferrites exhibit 42 vibrational modes in which 3 acoustic and 39 optical modes. There should be 5 active modes ($A_g + E_g + 3 F_{2g}$) should be observed in the Nickel ferrite [23, 24]. The Ag and Eg mode correspond to the symmetric elongation and symmetric bending of Fe-O and Ni-O bonds at the tetrahedral group site whereas F_{2g} (2), and F_{2g} (3) are asymmetric stretching and bending of Fe-O and Ni-O bonds at the octahedral site. In addition, the F_{2g} (1) mode is attributed due to the translational motion of the tetrahedral group. Notable is that modes A_g, E_g, and F_{2g} (3) display negligible metal atom displacement. [25] We have assigned 5 distinct Raman modes as shown in Figure 5, however, there might be multiple Raman modes possible. The experimentally obtained Raman modes (Table 4) align with those reported for single crystalline $NiFe_2O_4$, indicating consistency [26] and validating the XRD results. The slight shift of the Raman peaks for $Ni_{0.5}Al_{0.5}Fe_2O_4$ towards higher wave number values compared to $NiFe_2O_4$.

3.3 Fourier Transformer Infrared Spectroscopy (FTIR)

The recorded FTIR spectra for the synthesized samples are shown in Figure 6. Since spinel ferrites have four IR active bands that are shown as $4F_{1u}$ They are in the spectral region v_1 (630-560 cm^{-1}), v_2 (525-390 cm^{-1}), v_3 (380-335 cm^{-1}) and v_4(300-200 cm^{-1}). Two of the bands reported and found in the far-IR region have not been observed [27]. The FTIR investigations of the Ni-Al ferrite samples revealed the presence of two prominent absorption bands. One of these bands was attributed to the stretching vibration mode of metal-oxygen bonds in the tetrahedral sites, while the other band was assigned to octahedral group complexes, which is a characteristic feature of spinel ferrites [28].

In the case of the pure Nickel ferrite sample, two prominent absorption bands corresponding to metal-oxygen (Fe-O) stretching vibrations were observed at (424 cm^{-1} and 601 cm^{-1}) while (454.01 cm^{-1} and 619.3 cm^{-1}) in sample ($Ni_{0.5}Al_{0.5}Fe_2O_4$). These bands can be associated with the stretching vibration frequencies of metal-oxygen bonds in the octahedral and tetrahedral sites, respectively [29, 30]. The disparity in the band positions between the tetrahedral and octahedral complexes can be explained by the variation in the (Fe^{3+}–O^{2-}) bond distances. Furthermore, a comparison of the spectra of the synthesized samples indicated that the presence of additional modes in the aluminium substituted nickel ferrite sample could be attributed to the existence of impurities such as Fe_2O_3 [28].

TABLE III. Geometric parameters of $Ni_{1-x}Al_xFe_2O_4$ prepared samples. ρ denotes density in (g/cm^3), D denotes crystallite size in nanometers, A is the specific surface area in m^2/g, and d denotes bond length in Å.

x	Lattice constant (Å)	Volume (Å^3)	ρ	D	A	d (Ni-O)	d (Fe^{+2}-O)	d (Ni-Ni)	d (Fe-Fe)
0.0	8.34 ±0.004	580.09 ± 0.04	5.364	57	21.677	2.047 ±0.003	1.872± 0.003	3.611± 0.004	3.458 ± 0.002
0.5	8.27 ± 0.005	566.26 ± 0.01	5.189	46	25.174	2.028±0.034	1.863± 0.002	3.594 ± 0.002	3.441± 0.004
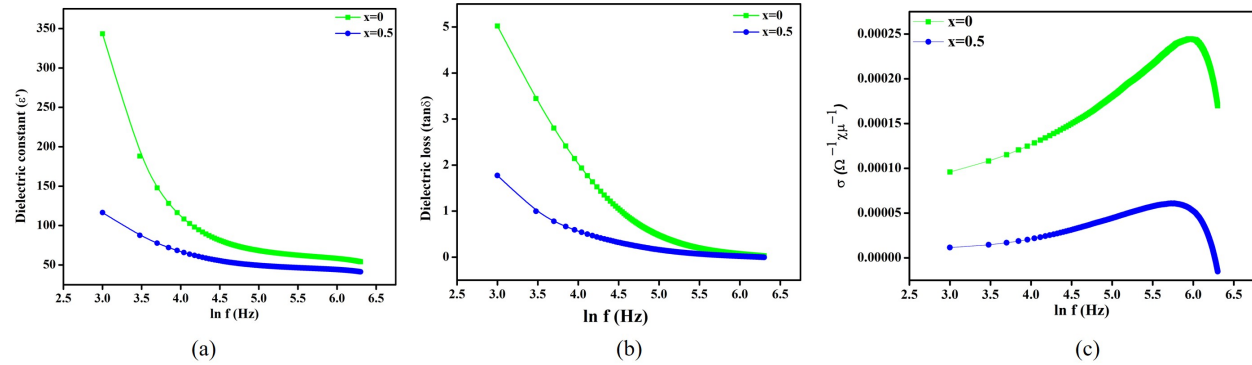
FIGURE 7. The variation of (a) dielectric constant, (b) dielectric loss and (c) AC conductivity with frequency of $Ni_{1-x}Al_xFe_2O_4$ (a) $x = 0$, (b) $x = 0.5$ at room temperature.

TABLE IV. Parameters calculated from Raman spectra of $Ni_{1-x}Al_xFe_2O_4$ ($x = 0, 1/2$) ferrite by using intense peaks.

Modes($\downarrow$)	Sample ($\rightarrow$)	NiFe$_2$O$_4$	Ni$_{0.5}$Al$_{0.5}$Fe$_2$O$_4$
		Raman Shift (cm^{-1})	
F_{2g}(1) (translational motion)	Tetrahedral Group Site	210±1	212± 1
E_g (symmetric bending)	Tetrahedral Group Site	333±1	334± 1
F_{2g}(2) (asymmetric stretching)	Octahedral Group Site	480±1	486± 1
F_{2g}(3) (asymmetric bending)	Octahedral Group Site	567 ±1	571 ± 1
A_g (symmetric stretching)	Tetrahedral Group Site	702 ±1	703 ± 1

3.4 Dielectric Study

Figure 7 (a-c) shows the variation of dielectric constant (ε'), tangent loss ($\tan\delta$), and ac conductivity with applied field frequency in a range of 1kHz -2MHz and observed frequency-dependent phenomena for the prepared samples. Both ε' and $\tan\delta$ shows dispersion with frequency i.e. the values of ε' and $\tan\delta$ are high at low frequency and then decreases rapidly with the rise in frequency. Ultimately, it attains a constant value which indicates the normal behavior of ferrites [15, 31]. This dielectric dispersion possibly depends upon two factors: (i) Electron hopping between Fe^{2+} and Fe^{3+} ions; (ii) Space charge polarization due to the presence of an inhomogeneous dielectric structure. The explanation for the high dielectric and loss values at lower frequencies lies in Koops' assumption [32], which posits that the ferrites generally consist of grains and grain boundaries, where the resistivity of grain boundaries is larger than the resistivity of grains which leads to the accumulation of charges at the interfaces between grains and grain boundaries. That charge contributes to the polarization and consequently to the ε' and $\tan\delta$ is high at low frequencies. Whereas, at high frequencies, most of those charges cannot follow the variation of the field and therefore their contribution to the polarization ceases. Therefore, ε' and $\tan\delta$ decreases with rise in frequency and reaches almost constant value as are observed [33, 34]. We observed low dielectric loss in $Ni_{0.5}Al_{0.5}Fe_2O_4$ compared to NiFe$_2$O$_4$. The low loss at higher frequencies suggests the potential applications of these materials in a high-frequency region.

An AC conductivity increases with the increase in frequency, however further increase in frequency which decreases as shown in Figure 7 (c). The conduction mechanism in ferrites is explained based on a hopping of electrons between Fe^{2+} and Fe^{3+} ions at octahedral sites [35]. As the frequency of an applied field increases, the hopping frequency of electrons enhances which causes an increase in the mobility of charge carriers. We observed a lower ac conductivity for $Ni_{0.5}Al_{0.5}Fe_2O_4$ than NiFe$_2$O$_4$ but followed the same pattern with frequency. The decrease in ac conductivity might be possible due to smaller grain size and higher grain boundaries in $Ni_{0.5}Al_{0.5}Fe_2O_4$ [36, 37].

4. CONCLUSION

Powder samples of $Ni_{1-x}Al_xFe_2O_4$ ($x = 0, 0.5$) have synthesized using sol-gel technique and studied the properties from the results of XRD, Raman, FTIR and dielectric measurements. Rietveld refinement of the XRD pattern confirmed the single cubic spinel phase purity of parent compound with Fd$\bar{3}$m space group. Lattice constant, volume, x-ray density and bond lengths were determined greater than the doped compound. This might be due to difference between ionic radii of Ni and Al. Crystallite

size using w-h method were found in the range of 45-60 nm. The cubic spinel symmetry also confirmed by the Raman and FTIR measurements. Five active modes of vibration were observed in the Raman analysis. FTIR investigations revealed the presence of two prominent absorption at tetrahedral and octahedral site, which might be attributed to the stretching vibration mode of metal-oxygen bonds. Dielectric constant (ε') and loss ($\tan \delta$) decrease as the frequency increases in both the samples. The low loss at higher frequencies suggested the potential applications of these materials in a high-frequency region. We observed a lower ac conductivity for $Ni_{0.5}Al_{0.5}Fe_2O_4$ than $NiFe_2O_4$ but followed the same pattern with frequency.

ACKNOWLEDGMENTS

EDITORS' NOTE

This manuscript was submitted to the Association of Nepali Physicists in America (ANPA) Conference 2023 for publication in the special issue of Journal of Nepal Physical Society.

REFERENCES

1. Y.-S. Borghei, S. Hosseinkhani, and M. Ganjali, "Engineering in modern medicine using 'magnetic nanoparticles' in understanding physicochemical interactions at the nano–bio interfaces," Mater. Today Chem **23**, 100733 (2022).

2. K. Wu, D. Su, J. Liu, R. Saha, and J.-P. Wang, "Magnetic nanoparticles in nanomedicine: a review of recent advances," Nanotechnol. **30**, 502003 (2019).

3. Y. Ren, Q. Dong, J. Feng, J. Ma, Q. Wen, and M. Zhang, "Magnetic porous ferrospinel $NiFe_2O_4$: A novel ozonation catalyst with strong catalytic property for degradation of di-n-butyl phthalate and convenient separation from water," J. Colloid Interface Sci. **382**, 90 (2012).

4. M. H. Jameel, M. Agam, M. Hamzah, S. Sufi, S. Rizvi, and J. Yabagi, "Structural, optical and morphological properties of zinc-doped cobalt-ferrites $CoFe_{2-x}Zn_xO_4$ ($x = 0.1 - 0.5$)," Dig. J. Nanomater. Biostructures **16**, 399 (2021).

5. L. Phor, S. Chahal, and V. Kumar, "Zn^{2+} substituted superparamagnetic $MgFe_2O_4$ spinel-ferrites: Investigations on structural and spin-interactions," J. Adv. Ceram **9**, 576 (2020).

6. N. Rajput, "Methods of preparation of nanoparticles-a review," Int. J. Adv. Eng. Technol. **7**, 1806 (2015).

7. A. E. Danks, S. R. Hall, and Z. Schnepp, "The evolution of 'sol–gel' chemistry as a technique for materials synthesis," Mater. Horiz. **3**, 91 (2016).

8. M. Z. Khan, I. H. Gul, M. M. Baig, and A. N. Khan, "Comprehensive study on structural, electrical, magnetic and photocatalytic degradation properties of Al^{3+} ions substituted nickel ferrites nanoparticles," J. Alloys Compd. **848**, 155795 (2020).

9. A. R. Chavan, S. D. Birajdar, R. R. Chilwar, and K. Jadhav, "Structural, morphological, optical, magnetic and electrical properties of Al^{3+} substituted nickel ferrite thin films," J. Alloys Compd. **735**, 2287 (2018).

10. H. S. Aziz, R. A. Khan, F. Shah, B. Ismail, J. Nisar, S. M. Shah, A. Rahim, and A. R. Khan, "Improved electrical, dielectric and magnetic properties of Al-Sm co-doped $NiFe_2O_4$ spinel ferrites nanoparticles," Mater. Sci. Eng.: B **243**, 47 (2019).

11. L. Kumar and P. Kumar, "Effect of Non Magnetic Substitution on the Structural and Magnetic Properties of Spinel Cobalt Ferrite ($CoFe_{2-x}Al_xO_4$) Ceramics," J. Mater. Sci.: Mater. Elect. **24**, 2706 (2013).

12. S. Greenwald, S. J. Pickart, and F. H. Grannis, "Cation Distribution and g Factors of Certain Spinels Containing Ni^{++}, Mn^{++}, Co^{++}, Al^{+++}, Ga^{+++}, and Fe^{+++}," J. Chem. Phys. **22**, 1597 (1954).

13. A. T. Raghavender, R. Kulkarni, and K. Jadhav, "Magnetic Properties of Nanocrystalline Al Doped Nickel Ferrite Synthesized by the Sol-Gel Method," Chin. J. Phys. **46**, 366 (2008).

14. H. R. Ebrahimi, M. Parish, G. R. Amiri, B. Bahraminejad, and S. Fatahian, "Synthesis, Characterization and gas sensitivity investigation of $Ni_{0.5}Zn_{0.5}Fe_2O_4$ nanoparticles," J. Magn. Magn. Mater. **414**, 55 (2016).

15. A. Bhosale and B. Chougule, "Electrical conduction in Ni–Al ferrites," Mater. Lett. **60**, 3912 (2006).

16. S. A. Lone, M. A. Dar, A. Kumar, P. Sharma, and D. Varshney, "Effect of Zn doping on structural and dielectric properties of tetragonal Nisub 1-xZnsub xFesub 2Osub 4 ($0.0 \leq x \leq 0.5$)," AIP Conf. Proc. **1665** (2015).

17. R. J. Hill and H. D. Flack, "Use of the durbin-watson d statistic in rietveld analysis," J. Appl. Cryst. **20**, 356 (1987).

18. B. H. Toby, "R factors in rietveld analysis: How good is good enough?" Powder Diffr. **21**, 67 (2006).

19. B. Rajesh Babu and T. Tatarchuk, "Elastic properties and antistructural modeling for nickel-zinc ferrite-aluminates," Mater. Chem. Phys. **207**, 534 (2018).

20. T. Ramesh and S. R. Murthy, "Electromagnetic properties of nanocrystalline Al^{3+} substituted MgCuMn ferrites synthesized by microwave hydrothermal method," Bull. Mater. Sci. **39**, 1593 (2016).

21. M. K. Bhattarai, S. P. Pavunny, and R. S. Katiyar, "Effect of La and Sc co-doping on dielectric and ferroelectric properties of PZT for energy storage capacitors," J. Appl. Phys. **130**, 034103 (2021).

22. P. S. Aghav, V. N. Dhage, M. L. Mane, D. R. Shengule, R. G. Dorik, and K. M. Jadhav, "Effect of aluminum substitution on the structural and magnetic properties of cobalt ferrite synthesized by sol–gel auto combustion process," Phys. B: Condens. Matter. **406**, 4350 (2011).

23. G. Dixit, J. P. Singh, R. C. Srivastava, H. M. Agrawal, and R. J. Chaudhary, "Structural, magnetic and optical studies of nickel fer-

rite thin films," Adv. Mater. Lett. **3**, 21 (2011).

24. P. Galinetto, B. Albini, M. Bini, and M. C. Mozzati, "Raman spectroscopy in zinc ferrites nanoparticles," Raman Spect. **1**, 223 (2018).

25. P. Graves, C. Johnston, and J. Campaniello, "Raman scattering in spinel structure ferrites," Mater. Res. Bull. **23**, 1651 (1988).

26. A. Ahlawat, V. Sathe, V. Reddy, and A. Gupta, "Mossbauer, Raman and X-ray diffraction studies of superparamagnetic $NiFe_2O_4$ nanoparticles prepared by sol–gel auto-combustion method," J. Magn. Magn. Mater. **323**, 2049 (2011).

27. R. Malekfar, M. Parishani, and A. a. Cheraghi, "Spectroscopy, Structural, and Optical Investigations of $NiFe_2O_4$ Ferrite," Int. J. Opt. Photonics **9**, 73 (2015).

28. M. Parishani, M. Nadafan, Z. Dehghani, R. Malekfar, and G. Khorrami, "Optical and dielectric properties of $NiFe_2O_4$ nanoparticles under different synthesized temperature," Results Phys. **7**, 3619 (2017).

29. M. Khairy and M. Gouda, "Electrical and optical properties of nickel ferrite/polyaniline nanocomposite," J. Adv. Res. **6**, 555 (2015).

30. R. Sen, P. Jain, R. Patidar, S. Srivastava, R. Rana, and N. Gupta, "Synthesis and Characterization of Nickel Ferrite ($NiFe_2O_4$) Nanoparticles Prepared by Sol- Gel Method," Mater. Today: Proc. **2**, 3750 (2015).

31. M. Darwish, A. Trukhanov, O. Senatov, A. Morchenko, S. Saafan, K. Astapovich, S. Trukhanov, E. Trukhanova, A. Pilyushkin, A. Sombra, D. Zhou, R. Jotania, and C. Singh, "Investigation of ac-measurements of epoxy/ferrite composites," Nanomater. **10**, 492 (2020).

32. C. G. Koops, "On the dispersion of resistivity and dielectric constant of some semiconductors at audiofrequencies," Phys. Rev. **83**, 121 (1951).

33. K. Iwauchi, "Dielectric Properties of Fine Particles of Fe_3O_4 and Some Ferrites," Jpn. J. Appl. Phys. **10**, 1520 (1971).

34. R. Nongjai, S. Khan, H. Ahmad, I. Khan, and A. Kandasami, "Magnetic and electrical properties of in doped cobalt ferrite nanoparticles," J. Appl. Phys. **112**, 084321 (2012).

35. S. Gangatharan, V. Chidambaram, and K. Sivakumar, "Synthesis, structural and dielectric studies of nickel substituted cobalt-zinc ferrite," Mater. Sci. Appl. **01**, 19 (2010).

36. M. A. El Hiti, "Dielectric behaviour in Mg-Zn ferrites," J. Magn. Magn. Mater. **192**, 305 (1999).

37. A. Farea, S. Kumar, K. Batoo, Y. Ali, C. G. Lee, and A. Alimuddin, "Structure and electrical properties of $Co_{0.5}Cd_xFe_{2.5-x}O_4$ ferrites," J. Alloys Compd. **464**, 361 (2007).